https://doi.org/10.1016/j.conbuildmat.2023.130760

Alkali-Activated Materials Partially Activated Using Flue Gas Residues: An Insight into Reaction Products

Muhammad Riaz Ahmad[1], Mehran Khan[1], Aiguo Wang[2], Zuhua Zhang[3], Jian-Guo Dai[1]*

Email: cejgdai@polyu.edu.hk (corresponding author)

1. Department of Civil and Environmental Engineering, The Hong Kong Polytechnic University, Hung Hom, Kowloon, Hong Kong
   Email: cejgdai@polyu.edu.hk (corresponding author)
2. Anhui Province Engineering Laboratory of Advanced Building Materials, Anhui Jianzhu University, Hefei 230601, China
3. Key Laboratory for Green & Advanced Civil Engineering Materials and Application Technology of Hunan Province, College of Civil Engineering, Hunan University, Changsha, PR China

Highlights

Flue gas residues (FGR) was utilized as alkaline activator

Reaction products were examined by selective dissolution approach

FGR could successfully replace the commercial activator in the AAFS pastes

N-A-S-H and C-A-S-H gels were main reaction products of AAFS pastes

Alkali-Activated Materials Partially Activated Using Flue Gas Residues: An Insight into Reaction Products

Abstract:

This study explored the feasibility of using flue gas residues (FGR) and commercial sodium silicate (CSS) as hybrid activators (HA) to prepare alkali-activated materials (AAMs). The CSS was replaced by 8, 16, and 24% FGR for a fixed amount of Na_2O. Results from selective dissolution techniques showed that control paste (CP-0F, 0% FGR) contained a slightly higher amount of N-A-S-H gel as compared to pastes prepared by hybrid activators (HAPs), whereas the amount of C-A-S-H gel was higher in HAPs containing 16% and 24% FGR. These findings were further corroborated by SEM-EDS analysis results. TGA, XRF and SEM-EDS analysis on paste residues confirmed the efficacy of HCl and SAM dissolution approaches to selectively dissolve the reaction products (N-A-S-H and C-A-S-H gels). SEM-EDS analysis showed that calcium-rich cross-linked gel (C-(N)-A-S-H) was present in all pastes. The gradual increase in reaction products of AAFS pastes with the increase in curing age was observed by XRD analysis. The ^{29}Si MAS NMR analysis revealed the formation of a higher amount of Q^4(0Al) and Q^4(1Al) species in HAPs as compared to control paste however a decline in the amount of Q^4(3Al) and Q^4(4Al) species was observed.

Keywords

Selective dissolution; Nuclear magnetic resonance; flue gas residue; alkali-activated gel; microstructure; reaction products

1 Introduction

Alkali-activated materials (AAMs) are considered as a suitable alternative cementitious material to OPC because of their sustainable nature that is beneficial in terms of low carbon emission and protection of natural resources. AAMs are produced when precursor materials react with an alkali metal (e.g., sodium silicate) in the presence of water [1–4]. Fly ash (FA) and ground granulated blast furnace slag (GGBS) are the most utilized precursors due to their availability and chemical stability [5–8]. The calcium source is

provided by the alkali-activated fly ash/slag (AAFS) binder in the form of GGBS, which not only produces calcium-rich alkali-activated gel (C-A-S-H) but also contributes to the formation of cross-linked N-C-A-S-H gel by partially replacing the Na from the geopolymer gel (N-A-S-H), indicating a higher degree of cross-linking between the reaction products [9–12].

When FA and GGBS are employed as precursors, alkali hydroxides in conjunction with alkali silicates (either potassium or sodium) have been widely investigated as alkaline activators because they form AAMs with superior mechanical properties [13–18]. However, there are some disadvantages of using alkali hydroxides and silicates, such as (a) they pose health and safety concerns owing to their highly alkaline solution nature, making them difficult to manage on-site; (b) activators, especially sodium silicate, that is usually produced by melting silicon dioxide and sodium carbonate around 1200-1400°C, release a huge amount of carbon dioxide, resulting in a negative environmental impact and costly activators having high embodied energy [19]. Regardless of high carbon emission from activators, previous research on AAMs has already shown that for an equivalent strength performance, the carbon emissions of AAM-based concretes are lower by 44-64% as compared to carbon emission of OPC concrete. Commercial alkali hydroxide and silicate-based activators are responsible for about 60% of total carbon emissions of AAMs [1,2,20]. Therefore, the scientific community is motivated to develop cost-effective alkaline activators with minimal environmental impact so that sustainability in the production of AAMs is further enhanced.

Several studies have been reported the manufacturing of sodium silicate activators from waste materials. Most of these studies employed sodium hydroxide as an alkali metal source and an amorphous silica-rich source to synthesize sodium silicate. The hydrothermal and thermochemical synthesis are commonly used methods to prepare alternative alkaline activators. Hydrothermally prepared activators need an elevated temperature in the range of 150-250°C of the pressure reactor vessel to increase the silica dissolution [21] and corrosive nature of activators may result in vessel damage. At low temperatures < 100°C, the dissolution of silica is very low and hence, the strength of AAMs prepared with such activators is likewise remarkably low [22,23]. The activators synthesized by the hydrothermal process can decrease carbon-

related emissions of AAMs up to 70% as compared to OPC concrete, however, the cost of producing AAMs is still higher than that of OPC concrete [24]. Alternative activators manufactured thermochemically needs the mixing of NaOH and glass powder at extremely high temperatures in the range of 500-1300°C. This approach can dissolve a higher amount of silica but requires reheating of synthesized activator for an hour at 175°C before using due to its partial solubility at room temperature [25–27].

Compared to the other techniques, activators synthesized from sand/waste glass powder and NaOH are deemed more practicable because it involves one-time mixing and heating of powders at 320°C for one hour. This technique generates a low-cost activator powder with a reduced carbon footprint [28]. Additionally, several studies have also described the synthesis of alternative activators utilizing NaOH in combination with a cleaning solution (CS), a waste from the alumina industry [29], bottom ash [30], sugar cane straw ash [31], waste glass [26,28,32], rice husk ash and silica fume [33].

Incineration technology is considered an effective way to reduce to volume of MSW and sewage sludge (85-90% reduction in waste volume) at waste-to-energy (WtE) plants. Hong Kong has one of the world's largest incineration sewage sludge plant (T.Park) and is also expected to complete its first MSW treatment plant (I.Park) by 2025 [34]. As Hong Kong government aims to achieve the net carbon footprint to zero in waste management, construction of more WtE facilities is expected so that MSW can be recycled into usable resources. Although, incineration technology greatly reduces the volume of wastes, ash residues which are produced after incineration are disposed to landfills. Hong Kong's landfills are about to run out of their storage capacity owing to land scarcity, and zero-landfill policy is going to be implemented since 2035. Therefore, it is of great importance to develop technologies to recycle such incineration residues to achieve the future sustainability goals.

FGR is a kind of industrial waste residue produced during the treatment of dewatered sewage sludge (SS) and municipal solid waste (MSW) at WtE facilities and is frequently disposed of in landfills [35]. The output of FGR is predicted to be between 2-6% of total waste burnt [36]. FGR is made up of fly ashes and particles collected during the flue-gas cleaning phase downstream of the gas treatment process. It is highly

corrosive and alkaline, being consisted of contaminants and soluble ions, and stored at the plant site temporarily. After that, it is disposed of in the landfills according to waste disposal regulatory requirements. Numerous standards classify FGR as a hazardous material [36,37]. Annual FGR output will continue to grow with the establishment of WtE facilities. Therefore, developing an alternate method of recovering/recycling this type of residues is essential.

It should be noted that a few studies on the application of FGR in civil engineering have been reported [38–40]. The precursors for the AAMs were developed by treating FGR with DC plasma technology and glass-forming additives [47,48]. A low-strength AAM (<10 MPa) was prepared through alkali activation by combining the FGR with co-fired fuel ash [43]. Solidification of high volume of FGR (80% of total weight) by geopolymerization technology and immobilization of heavy metals leaching was also successfully demonstrated in a recent study [35]. FGR manufactured in the Hong Kong WtE facility contains a high concentration of alkaline metals and can be utilized as a source of alkali-activators for activation of the aluminosilicate precursors and slags by partially replacing the commercial sodium silicate (CSS). Therefore, this research aims to investigate the use of hybrid activator containing CSS and FGR in the synthesis of one-part AAFS pastes to provide further insight into reaction mechanism in addition to our previous research [44]. To study the reaction products of HAPs and control paste, HCl and SAM based selective dissolution techniques were adopted. The ICP-OES analysis of filtrates and TGA, XRD, and SEM analysis on undissolved residues was also conducted to characterize the reaction products. The ^{29}Si MAS NMR study on AAFS pastes was performed to quantify the type of silicate structural units.

2 Materials and methods

2.1 Raw materials and properties

GGBS and sodium silicate were bought from China, and FA was supplied from Hong Kong's CLP power plant. FGR was sourced from the T-park incineration plant. FGR was dried in an oven at 105°C to eliminate any remaining moisture and then finely ground to powder for 4 hours in a ball mill. The particle size distributions of FGR, GGBS, and FA, were determined using the laser diffraction method, as shown in Fig.

1. FGR, GGBS, and FA had an average particle size of, 7.0 14.1, and 20.1 µm, respectively. The chemical composition of FGR, CSS, GGBS, and FA was determined using the X-ray fluorescence emission (XRF) technique and are provided elsewhere [44]. FA was categorized as low-calcium (Class F) FA as per ASTM C618-19. GGBS contains of Al_2O_3 (14.7%), SiO_2 (32.6%) and CaO (42.4%). CSS is composed of SiO_2 (46.3%) and Na_2O (50.7%), whereas FGR is composed of SO_3 (31.9%) and Na_2O (38.3%). FGR's chemical composition indicates that it includes a high concentration of alkali metals, which may aid in the activation of the aluminosilicate precursor. Additionally, the presence of SO_3 and Na_2O suggests a high concentration of Na_2SO_4 in FGR, which has been utilized as an alkaline activator in author previous research and literature [45,46].

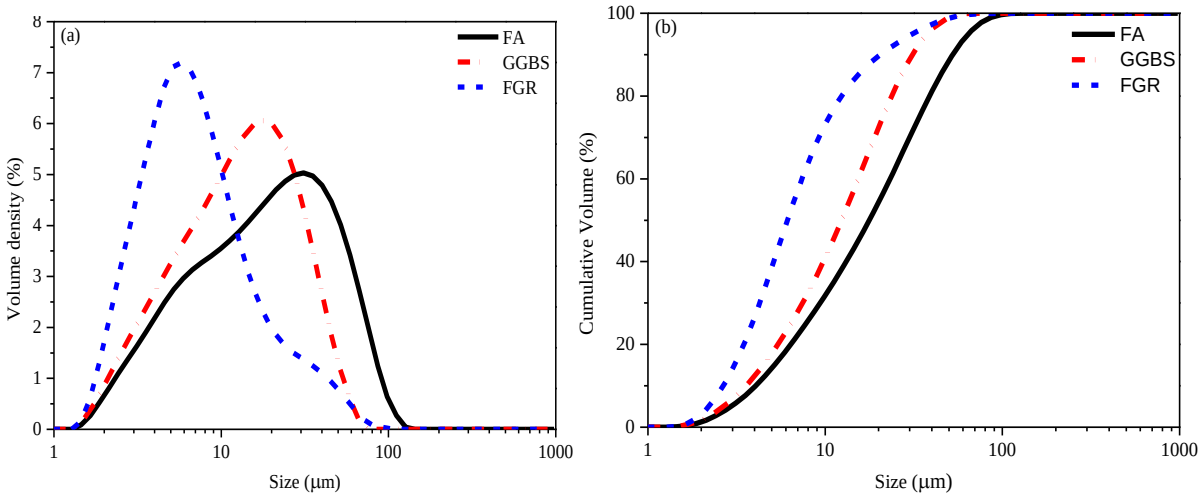

Fig. 1. Particle size distribution of FA, GGBS and FGR (a) volume density and (b) cumulative volume

Fig. 2 depicts SEM pictures of raw materials powders. FA is composed of spherical particles with a smooth surface. The shape of FGR particles is fluffy with partially curved edges, and GGBS particles are of angular shape.

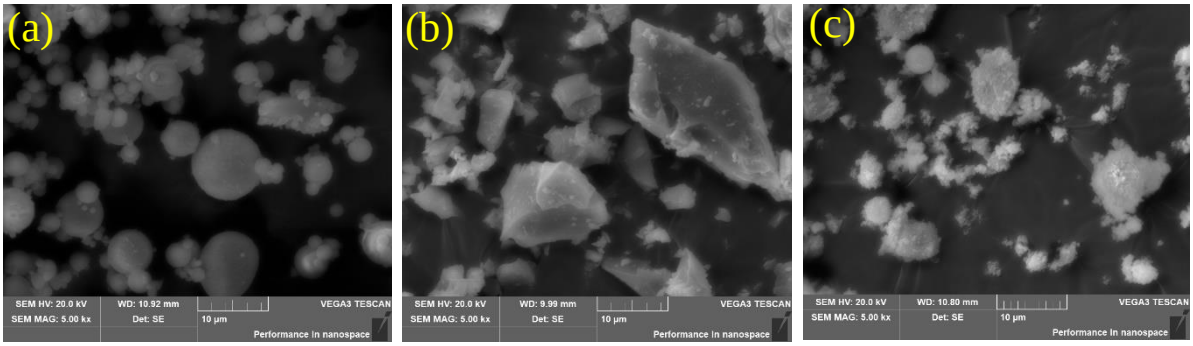

Fig. 2. Morphology of (a) FA, (b) GGBS and (c) FGR particles observed by SEM

2.2 Mixing and casting

The GGBS, FA, CSS, and FGR were used for the preparation of four AAFS pastes. For all mixes, the ratio of FA to GGBS was kept constant. The control mix (referred to CP-0F paste) was made by mixing the CSS with FA and GGBS and did not contain FGR. The CP-0F had a CSS/binder ratio of 0.12 (Na_2O/binder = 6.1%). For the other combinations, CSS was replaced by 8%, 16%, and 24% FGR, by mass denoted as HAP-8F, HAP-16F, and HAP-24F (HAPs; pastes activated by hybrid activators CSS and FGR) respectively. The FGR was added so that the alkali content to binder ratio remained constant (Na_2O/binder = 6.1%) for all pastes. The mix proportions of AAFS-pastes are kept same as our previous research work [44]. CSS includes some silica that is readily soluble and can contribute to the early strength of AAFS pastes whereas no additional silica source was added to mixes containing FGR. As a result of the inclusion of FGR, the modulus ratio of the activator was slightly reduced. To make the AAFS pastes, all raw components were dry mixed for 5 minutes in a Hobart mixer. Following that, water was added to the dry mixes and blended for 2 minutes at a low speed. Finally, mixing was maintained at a high speed for an additional 3 minutes to produce a homogenous slurry. Fresh AAFS pastes were poured into 40 mm^3 cubic molds, then vibrated for 1 minute, and finally covered with plastic sheets to avoid moisture loss. After 24 hours, samples were removed from the molds and kept at room temperature.

2.3 Testing methods

The effect of FGR on the mechanical performance and microstructure of AAFS paste was studied. Through a selective dissolution procedure, gel composition of AAFS pastes and reaction extent of activator was

studied. The hydration of samples was stopped prior to selective dissolution by immersing in ethanol for 7 days and drying in a vacuum oven at a constant temperature of 40°C. Salicylic Acid/Methanol (SAM) extraction of AAFS paste was carried out by dissolving 2 g of AAFS paste and raw materials in a SAM solution comprising 8 g salicylic acid and 120 ml methanol. A magnetic stirrer was used to stir the mixture for 3 hours, and the suspension was filtered using a Whatman filter (0.2 um pore size) and a Buchner funnel under vacuum conditions. The methanol-washed insoluble residues were dried in an oven, weighed, and stored in a vacuum desiccator. SAM extraction of AAFS paste dissolves the C-(A)-S-H gel and does not dissolve the geopolymer gel (N-A-S-H) or unreacted precursors (GGBS and FA) [12]. HCl extraction was used to dissolve the geopolymer gel (N-A-S-H gel and zeolite). During this process, silica gel and unreacted FA are left as insoluble residues [12]. However, HCl extraction can also decompose C-S-H/C-A-S-H gel by dissolving the Ca^{+2} and leaving the silica gel behind. This method can completely dissolve the raw slag. The HCl extraction was carried out by dissolving 1 gram of AAFS paste in 250 ml of HCl (1:20). The mixture was stirred for 3 hours using a magnetic stirrer and filtered using a vacuum pump. The insoluble residues were neutralized with deionized water, dried in an oven, weighed, and stored in a vacuum desiccator. The alkaline activator's reactivity was determined by dissolving the AAFS pastes (2 g) in distilled water (200 g) for 3 hours at a temperature of 25°C in an ultrasonic bath. Afterward, all the mixtures were filtered and the insoluble residues were oven-dried and weighed. Finally, they were stored in a vacuum desiccator. Filtrates were stored at -4°C for the Inductively Coupled Plasma-Optical Emission Spectrometer (ICP-OES, SpectroBlue ICP-OES) analysis. For ICP-OES analysis, filtrates were digested with the concentrated HNO_3 (sample 5:2 HNO_3), diluted with 5% HNO_3, and run for ICP-OES analysis. The original paste powders, HCl residues and SAM residues were tested for the TGA, XRF, and SEM analysis.

Hydration of samples for the TGA, XRF, and XRD and SEM analysis was also stopped at 28 days by immersing them in ethanol for 7 days and followed by drying in a vacuum oven. Samples for TGA, XRF and XRD were grinded into fine powder by a mortar and pestle. The powder samples were then sieved through the mesh size 200 (<75 µm). Rigaku Thermo Plus EVO2 equipment was used to conduct

thermogravimetric analysis (TGA) on AAFS paste powder samples. Each paste powder sample weighed around 15 mg. A constant heating rate of 10°C/min was maintained throughout the heating of all powder samples from 30-1000°C. The TGA analysis was performed on the original paste powders, SAM residues, and HCl residues. The chemical composition of original AAFS paste powder, HCl residues, and SAM residues was determined by Rigaku Supermini200 XRF equipment. XRF pellets were prepared by placing the powders samples in pellet die with the sublayer of boric acid. The samples were compressed using the automatic compression machine and prepared pellets were analyzed for chemical composition. XRD patterns were measured using Rigaku SmartLab-Advance machine. The testing conditions for all samples were kept constant as follows; current 200mA, voltage 45kV, scanning step 0.02°, and focusing mode Bragg-Brentano. The samples for XRD were tested after 7 and 28 days of hydration age.

The hydration products of AAFS pastes were studied using a scanning electron microscope (SEM, Tescan Vega 3 XMU) equipped with an EDS facility. The dried AAFS paste samples were embedded in an epoxy resin under vacuum conditions. Samples were extracted from molds after hardening of epoxy and polished using a Buehler (AutoMet 300) polisher. The grinding of epoxy was carried out using Grit 600 and water as a lubricant until the surface of samples is exposed. After that, the samples were polished for 5 minutes for each grit to obtain a smooth surface using the MetaDi diamond suspensions (9µm, 5µm, and 0.05µm diamond/alumina grits) respectively. The attached particles to the surface of samples were removed by submerging the samples in ethanol in an ultrasonic bath during the grinding and polishing when changing the different grits. After polishing, samples were dried in a vacuum oven, sputtered with a thin gold layer, and analyzed using SEM-EDS. SEM examination was conducted in a high vacuum environment using backscattered electron (BSE) imaging mode at a working distance of 15.0 mm and an accelerated voltage of 25 keV.

Solid state ^{29}Si NMR spectra of AAFS pastes samples were acquired using a Jeol ECZ500R Solid-state NMR (SSNMR) spectrometer to identify the chemical shifts of different structural units during the reaction. The ^{29}Si NMR spectra of pastes were obtained at a frequency value of 98.39 MHz while applying a spinning

speed of 4 kHz on a 8 mm MAS probe using field strength of 11.63 T. Single pulse experiment was performed by applying a pulse width of 5.0 μs and relaxation delays of 10 s. To obtain spectra with a good signal-to noise ratio, experimental times of about 20-24 h were necessary. A total of more than 5000 scans were recorded for each sample.

3 Results and Discussions

3.1 Selective dissolution and ICP-OES analysis

Dissolution of selective phases through the SAM extraction, HCl extraction, and water extraction (coupled with the ICP-OES analysis) was performed to study the amount of different reaction products and unreacted products [11,47]. The soluble phases are represented in terms of percentage of the total mass in Fig. 3. The percentage of dissolved reaction products (mainly C-A-S-H) through the SAM extraction for the AAFS pastes was very close to each other. The amount of C-A-S-H gel formed in the CP-0F paste was 46.9%, which was nearly the same as that in HAP-16F (46.4%) and HAP-24F (46.4%). A slightly lower amount of C-A-S-H gel (45.9%) was formed in the HAP-8F paste. Interestingly, these results are in line with the quantitative SEM-EDS point analysis (discussed in section 3.5) where the Ca/Si ratio (0.33) in HAP-8F was lowest as compared to other AAFS pastes (Ca/Si = 0.37-0.44).

HCl extraction is normally performed to study the dissolution of geopolymeric gel (N-A-S-H). However, it should be noted that HCl extraction also tends to dissolve Ca^{+2} based phases from the C-(A)-S-H gel. [12]. Hence, the amount of N-A-S-H gel was calculated by subtracting the SAM dissolution results from HCl dissolution results. The amount of N-A-S-H is slightly overestimated as unreacted GGBS could be also dissolved by HCl dissolution (the dissolution degree of unreacted GGBS in HCl in 98.24%), however this phenomenon is common in all four pastes and assumed to have minor influence on final results of reaction products. It can be observed that, the amount of geopolymer gel in the CP-0F (14.5%) and HAP-8F (16.3%) pastes were comparable to each other but higher than that of HAP-16F (11.5%) and HAP-24F (11.4%). These results also verified the SEM-EDS analysis (discussed in section 3.5) where the Na/Si and Na/Al ratios in CP-0F and HAP-8F gel pastes were also higher than that of HAP-16F and HAP-24F.

The extent of reaction of alkaline activators was accessed by the water extraction method and results are provided in Table 1. It has been reported that unreacted alkaline activators in the paste can dissolve in distilled water [48]. Hence, dissolution results from water extraction can be indirectly used to access the solubility of alkaline activator. It is noticeable that amount of unreacted alkaline activator was higher in the control AAFS paste (R-0) which showed the dissolution of 17.2% during water extraction. For the pastes containing 8, 16, and 24% FGR as replacement of CSS, unreacted alkaline activator was slightly declined as amount of dissolved alkalis was slightly reduced to 16.7, 16.4, and 15.2% respectively. Dissolution of raw precursors is also given in Table 1. FA and GGBS dissolved in water in lower quantities whereas dissolution of FGR was highest into the water among all the pastes and raw precursors due to the availability of alkali metals. This proved that FGR is readily dissolvable into water and can participate in chemical reaction like CSS.

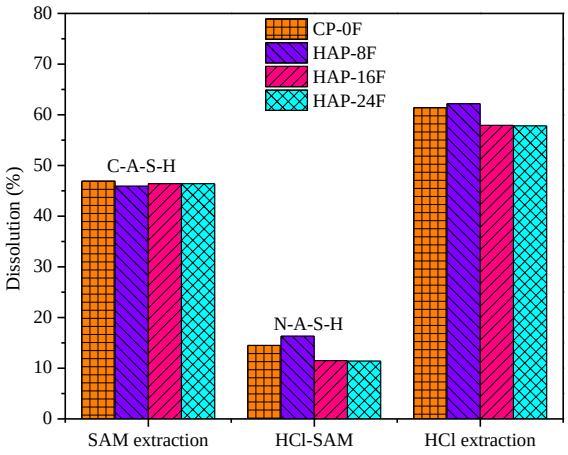

Fig. 3. Dissolution of reacted and unreacted phases through selective dissolution

Table 1. Dissolution of AAFS pastes and raw precursors into water

Sample ID	Dissolution into water (%)
CP-0F	17.2
HAP-8F	16.7
HAP-16F	16.4
HAP-24F	15.2
FA	5.1
GGBS	3.5
FGR	73.6

The leaching concentration of calcium-rich gel (C-A-S-H) elements (Ca, Al and Si) by SAM extraction determined by the ICP-OES analysis is shown in Table 2. The concentration of leaching concentration of Ca and Si was higher in HAP-16F and HAP-24F as compared to CP-0F, while HAP-8F showed a lower concentration of Ca, and Si as compared to CP-0F. It indicates that a higher amount of calcium-rich C-A-S-H gel was present in HAP-16F and HAP-24F pastes as compared to CP-0F and HAP-8F. The concentration of Al was highest in CP-0F and was followed by HAP-24F, HAP-16F, and HAP-8F. The release of a higher amount of Ca into solution is associated with the higher amount of Ca in pastes and lower dissociation energy of Ca-O bond as compared to Al-O and other bonds [49,50]. Similarly, a higher amount of Ca was released from the raw precursors.

The study of geopolymer gel (N-A-S-H) was conducted by dissolving the AAFS pastes in HCl solution (Table 2). As HCl can dissolve all the Ca^{+2} and 100% GGBS, the discussion on Ca leaching for HCl extraction is ignored. The leaching ratio of Na/Si for R-0, R-8, R-16, and R-24 were 1.09, 0.8, 0.92, and 0.88 respectively, suggesting that the control paste had a higher amount of geopolymer gel as compared to HAPs. The dissolved concentration of both Si and Al was gradually increased when CSS was replaced by 8, 16, and 24% with the FGR, this could be associated with the higher alkalinity of paste with the lower silicate modulus which helped to dissolve the more Al and Si elements from the precursors.

Table 2. The dissolved concentrations of Al, Ca, Na, and Si by SAM, HCl and Water dissolution methods (mg/L)

Dissolution method	Mix ID	Al	Ca	Na	Si
SAM	CP-0F	625	2959	521	749
	HAP-8F	465	2604	486	660
	HAP-16F	564	3517	710	892
	HAP-24F	591	3513	586	796
	FA	119	2421	334	323
	GGBS	304	3028	305	354
	FGR	26	565	389	132
HCl	CP-0F	204	2187	325	297
	HAP-8F	324	2318	347	434
	HAP-16F	336	2928	352	385
	HAP-24F	618	2336	373	425

	FA	222	2542	328	494
	GGBS	348	3828	316	433
	FGR	149	2213	583	244
Water	CP-0F	307	647	455	648
	HAP-8F	72	356	437	928
	HAP-16F	62	194	402	230
	HAP-24F	54	150	372	258
	FA	96	641	325	430
	GGBS	858	2063	326	376
	FGR	56	772	1031	247

The leaching concentration of elements (Ca, Al, Na, and Si) in water are given in Table 2. The leaching concentration of Ca was gradually decreased as CSS was replaced by FGR. This also means that unreacted Ca was higher in the control paste (CP-0F) as compared to HAP pastes. Similarly, the leaching concentration of Al was highest for the control paste, showing that a relatively lower quantity of Al in CP-0F paste had dissolved to form reaction products as compared to other pastes. The concentration of Na had marginal differences among all pastes. Dissolution of Ca was highest for the raw GGBS due to the presence of high calcium in its chemical composition, whereas dissolution of Na was highest in the FGR as it was one of the major components in FGR. It is important to mention that results from the selective dissolution of elements and leaching concentration of ICP analysis are in accordance with the results of SEM-EDS analysis (which are discussed in following section), as a slightly lower amount of Ca dissolution was observed in the control paste (CP-0F) in both analyses.

3.2 TGA analysis of original pastes and AAFS pastes residues

TGA analysis of original pastes powders and residues after HCl and SAM dissolution was conducted to study the reaction products. The mass loss for the raw materials and original paste powders is presented in Fig. 4a. The mass loss for the FA and GGBS is quite low. However, FGR showed significant mass loss beyond 600°C which is attributed to the evaporation and melting of soluble salts of FGR [35] [51]. For the AAM pastes, the mass loss at different temperatures is attributed to different reaction products. At a lower temperature below 150°C, the mass loss is linked to the evaporation of physically bound water [51–53]. The chemically bound water of geopolymer gel (N-A-S-H) is evaporated in the range of 150-300°C whereas

dehydration of alkali-activated gel (C-A-S-H) occurs in the range of 300-600°C. The loss in mass due to dehydration of reaction products is generally completed when temperature reaches 600°C. The loss in mass for the original paste powders CP-0F, HAP-8F, HAP-16F and HAP-24F up to 600°C was 10.71, 11.10, 11.86, and 12.22% respectively which indicates that a higher degree of reaction occurred in the mixtures containing FGR as partial replacement of CSS.

The TGA analysis was performed on the HCl and SAM residues and results of mass loss are presented in Fig. 4b and Fig. 4c respectively. As HCl treatment mainly dissolves geopolymer gel (N-A-S-H) and SAM treatment dissolves alkali-activated gel (calcium-rich phases), the residues of HCl and SAM are considered to be mainly consisted of C-A-S-H and N-A-S-H phases respectively along with the unreacted phases. The mass loss curves of HCl and SAM residues showed an opposite behavior to that of original paste powders. The mass loss of CP-0F residues was highest both for HCl and SAM treatment followed by the HAP-8F, HAP-24F, and HAP-16F. The mass loss for SAM residues in the range of 150-300°C is shown in Fig. 4d and is an indirect indication of presence of N-A-S-H gel in AAFS pastes. Higher mass loss for the CP-0F residue in this range shows that a relatively higher amount of N-A-S-H gel was formed in CP-0F as compared to pastes containing FGR. However, the presence of alkali-activated gel (C-A-S-H) in HCl residues showed minor variations among different AAFS pastes (300-600°C). The presence of C-A-S-H could be underestimated in by HCl residues as HCl dissolution could also dissolve significant amount of Ca^{+2} ions.

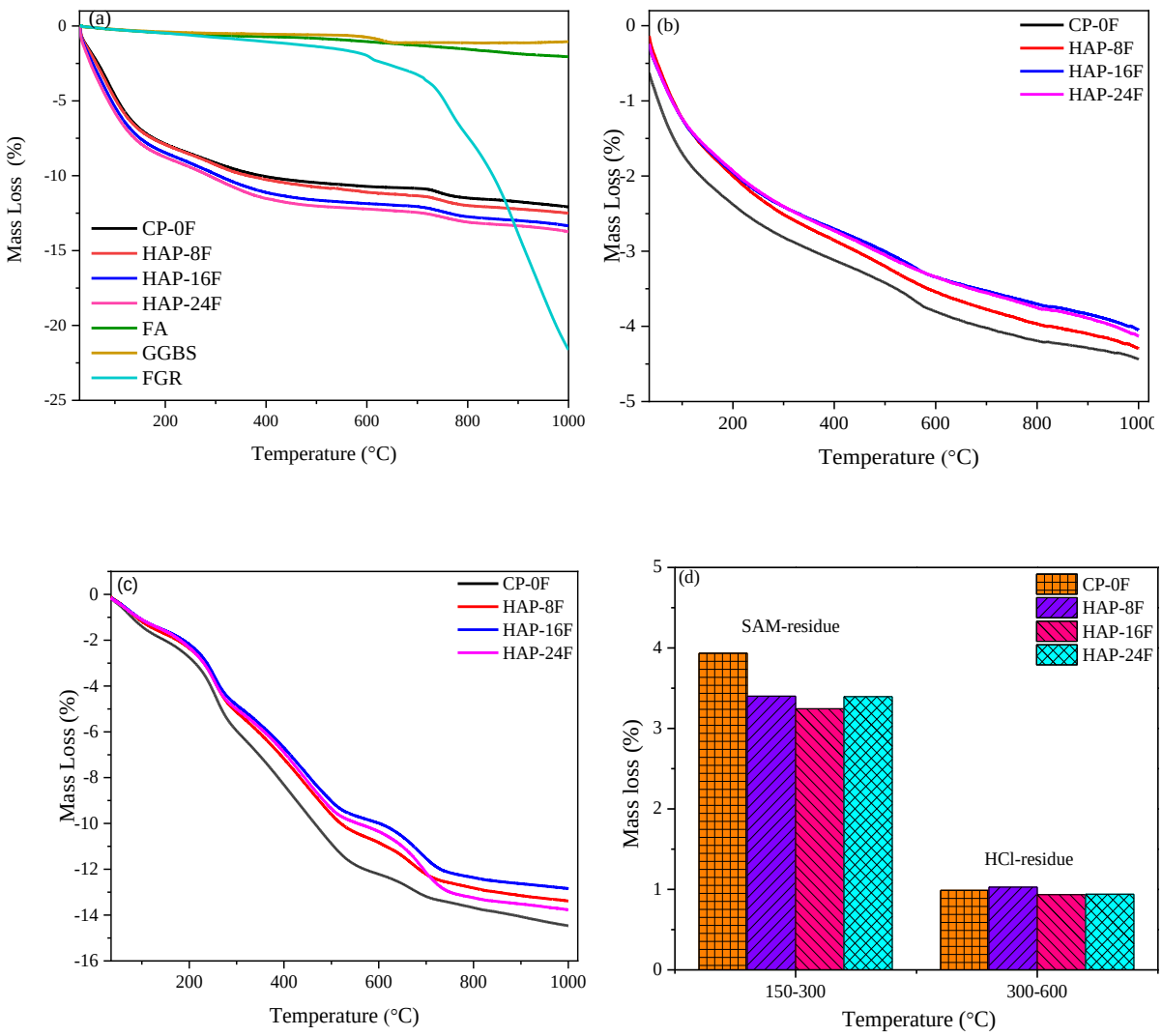

Fig. 4. TGA analysis of (a) original AAFS pastes; (b) residues of pastes after HCl selective dissolution; (c) residues of pastes after SAM selective dissolution and (d) mass loss of residues after SAM and HCl treatment in range of 150-300°C and 300-600°C respectively.

3.3 XRF analysis of original pastes and AAFS pastes residues

The original AAFS paste powders and insoluble residues after the HCl and SAM dissolution were analyzed by XRF analysis. The contents of Na_2O, CaO, SiO_2, and Al_2O_3 in original paste powders and insoluble residues are shown in Fig. 5. The formation of C-A-S-H gel is studied by the dissolution of Ca-based phases via SAM treatment. The control paste (CP-0F) showed the higher dissolution of CaO (34.6%) after SAM dissolution, which was followed by HAP-16F (28.9%), HAP-24F (25.5%), and HAP-8F (22.8%) respectively. As SAM treatment dissolves both CaO and Na_2O based phases during the dissolution process,

the co-existence of calcium-rich alkali-activated and geopolymer gels (C-N-A-S-H) is expected in all the AAFS pastes.

The percentage of remaining Na_2O and CaO in HCl-residues after HCl dissolution was significantly reduced in all mixtures. The complete dissolution of Na_2O is observed in HAP-8F and HAP-24F mixtures (Fig. 5a), which indicates the formation of a slightly higher amount of geopolymer gel (N-A-S-H) in these two pastes as compared to CP-0F and HAP-16F. The HCl treatment also influenced the Ca-based phases in the AAFS pastes (Fig. 5b) as it can also dissolve the Ca-based phases. The percentage of SiO_2 and Al_2O_3 after SAM and HCl dissolution was significantly increased than that of the original paste. The percentage of SiO_2 and Al_2O_3 in SAM-residue was highest for the reference paste (CP-0F), which indicates a slightly lower amount of FA reacted to form the C-A-S-H gel. The contents of unreacted SiO_2 and Al_2O_3 were further increased for HCl dissolution as HCl treatment can dissolve the Ca from the slag leaving behind SiO_2 and Al_2O_3. Hence, a higher amount of SiO_2 and Al_2O_3 in HCl-residue is due to the presence of unreacted Si and Al both from slag and FA. The nearly similar percentage of silica and alumina for all AAFS pastes in HCl and SAM residues shows that the reactivity of FA and slag differs slightly among different pastes, when FGR and CSS based hybrid activator is utilized.

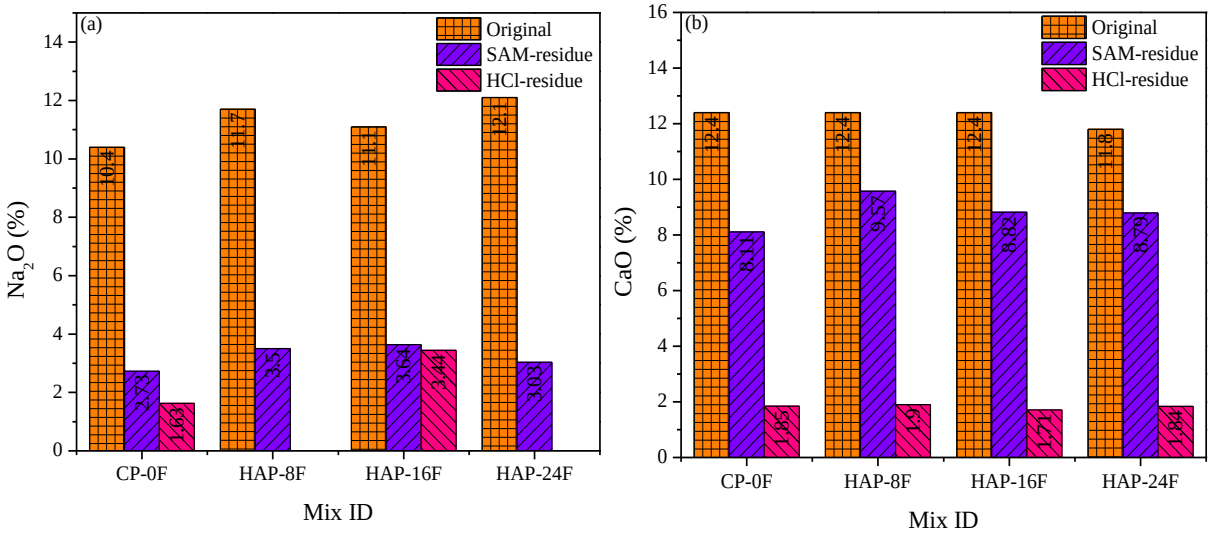

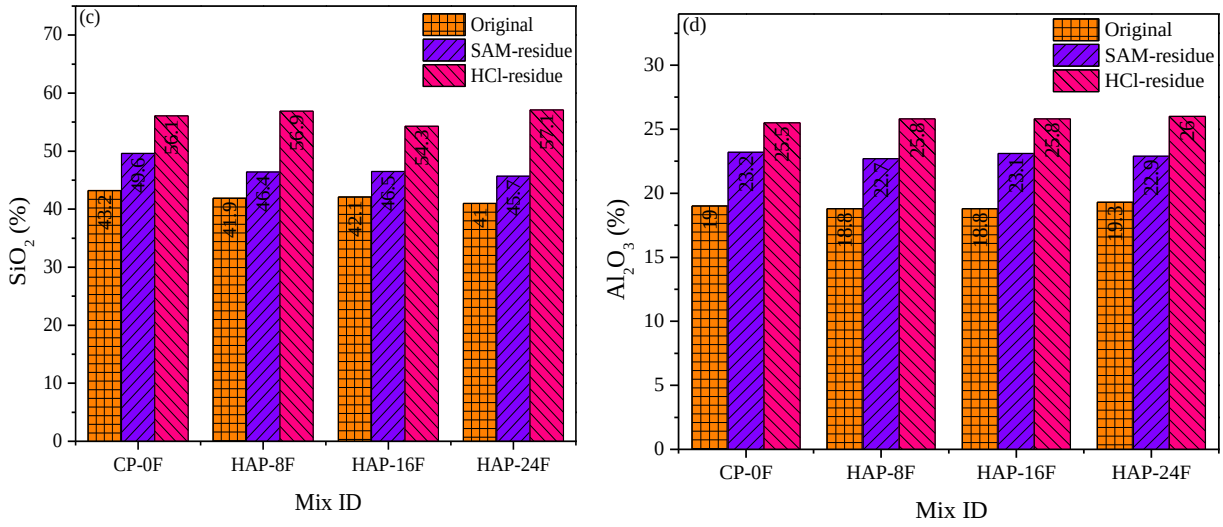

Fig. 5. Oxides composition for the AAFS pastes residues after HCl and SAM selective dissolution for (a) Na_2O; (b) CaO; (c) SiO_2 and (d) Al_2O_3

3.4 SEM-EDS analysis

3.4.1 SEM-EDS analysis of original paste, HCl residue, and SAM residue powders

SEM analysis on original paste powder and residues was performed to study morphology and chemical composition. The results are shown in Fig. 6 only for the mixture containing 24% FGR as a replacement of CSS (HAP-24F). The EDS point analysis was performed on the powder particles and the atomic percentages of elements are shown in Table 3. Morphology and chemical composition of residues showed considerable differences from the original paste powders. Original paste powder contained irregular particles with larger sizes (Fig. 6a). After HCl and SAM dissolution, the particle size of residues was reduced significantly. HCl-residues of HAP-24F mainly consist of sphere shapes particles which indicates that most of the reaction products were dissolved leaving behind the unreacted FA (Fig. 6b). SAM residues also consisted of a higher amount of FA particles as compared to the original paste powder (Fig. 6c). The change in morphology and particle size of residues is associated with the dissolution of reaction products.

The EDS point analysis was conducted on the powder samples to investigate the chemical composition. The point analysis on spot 1 (HAP-24F) shows the presence of Ca, Na, Si, and Al elements which are attributed to cross-linked gel (C-N-A-S-H). Spot 2 indicates the presence of partially reacted FA with a slightly lower Si/Al of 1.57 than that of raw FA (1.75) [44]. The partially reacted slag particle to form the

cross-linked gel can be observed in spot 3. After HCl dissolution, Na and Ca related phases (C-N-A-S-H) were quickly dissolved as a little amount of Na and Ca was detected after HCl dissolution (spot 4). The Ca/Si, Na/Si, Na/Al ratio was decreased from 0.35, 0.44 and 0.98 to 0.02, 0.02 and 0.03 respectively after HCl dissolution. This finding also agrees with the XRF results as discussed above. The composition of unreacted FA remained unchanged after dissolution (spot 5). However, Ca phases from unreacted slag particles were completely dissolved (spot 6) as Ca/Si was reduced to 0.02. The Ca/Si of raw slag powder is 1.99. SAM treatment prominently dissolved Ca-based phases however the amount of Na was also significantly reduced. This could be linked to the presence of cross-linked gel comprising of both Na and Ca, which was dissolved upon SAM treatment. The Ca/Si, Na/Si, Na/Al ratio was decreased from 0.35, 0.44 and 0.98 to 0.06, 0.06 and 0.26 respectively after SAM dissolution (spot 7). A higher ratio of Na/Al in SAM residue as compared to HCl residue indicates the remnant of geopolymer gel (N-A-S-H) formed in HAP-24F.

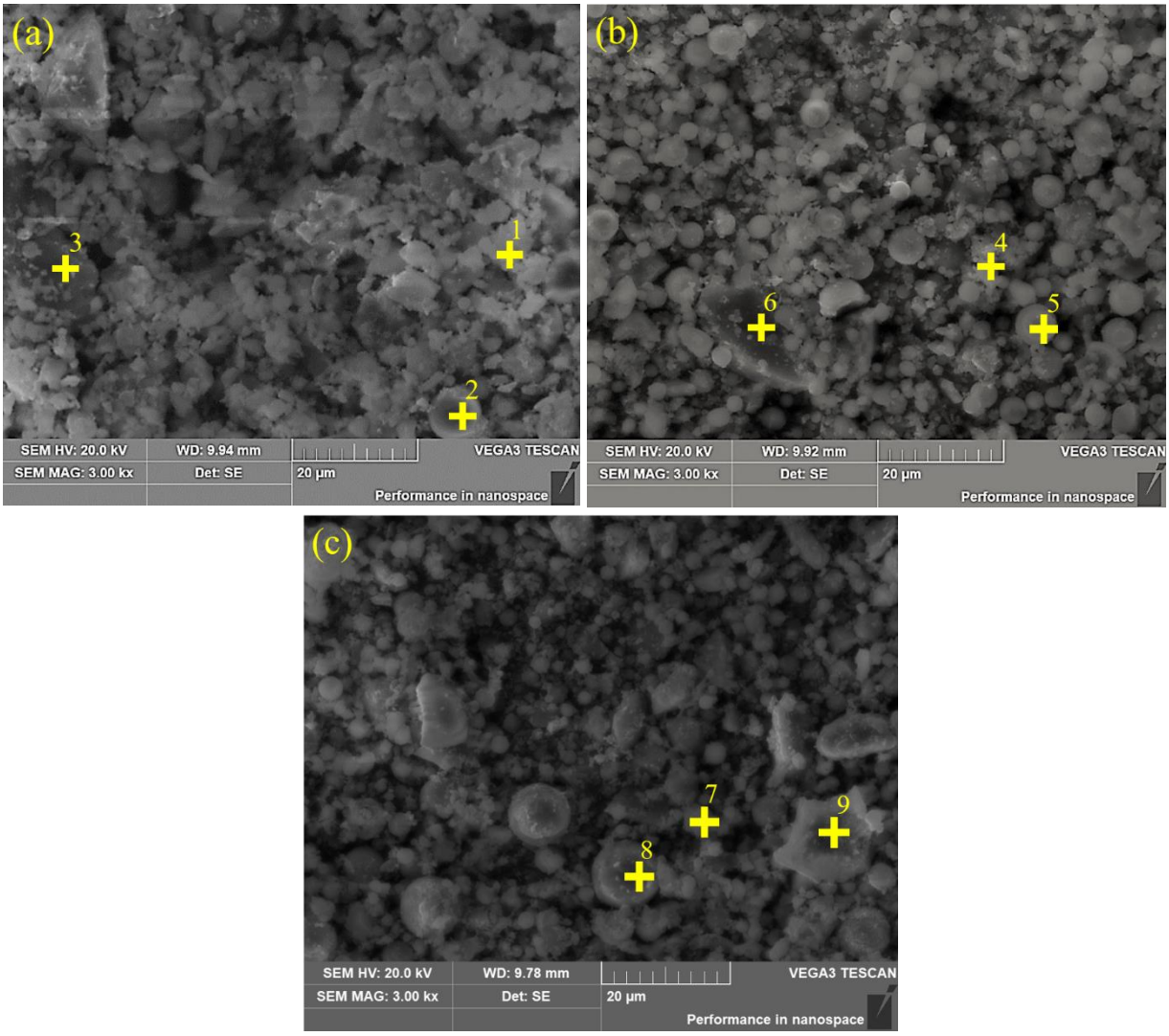

Fig. 6. SEM images for (a) original HAP-24F paste powder; (b) HCl residues of HAP-24F paste powder and (c) SAM residues of HAP-24F paste powder

Table 3. Elemental composition of HAP-24F paste powder and its residues

	Atomic percentage (%)								
	HAP-24F paste powder			HAP-24F HCl residue			HAP-24F SAM residue		
Elements	1	2	3	4	5	6	7	8	9
Na	18.0	4.9	10.3	1.2	2.4	3.7	3.9	5.7	2.5
Mg	4.3	3.9	1.5	1.3	2.4	2.9	2.7	2.4	3.3
Al	18.3	31.2	28.3	42.1	31.9	23.4	15.0	27.4	27.6
Si	41.0	48.9	45.4	51.0	50.1	62.1	67.9	55.7	58.6
K	1.1	2.7	1.7	1.2	3.4	4.4	3.2	3.9	3.6
Ca	14.2	4.2	10.1	0.8	1.5	1.1	4.0	1.2	2.0
Fe	3.1	4.3	2.7	2.4	8.4	2.4	3.4	3.7	2.4
Ca/Si	0.35	0.08	0.22	0.02	0.03	0.02	0.06	0.02	0.03
Na/Si	0.44	0.10	0.23	0.02	0.05	0.06	0.06	0.10	0.04
Si/Al	2.24	1.57	1.61	1.21	1.57	2.65	4.53	2.04	2.12
Na/Al	0.98	0.16	0.36	0.03	0.07	0.16	0.26	0.21	0.09

3.4.2 BSE-EDS analysis of AAFS pastes

The nature of reaction products of AAFS pastes was examined by the BSE-EDS analysis. The presence of different phases (unreacted FA, unreacted GGBS, partially and completely reacted FA, presence of gel, Fe particles) can be observed as shown in Fig. 7. The representative spectra for SEM-EDS point analysis on the main reaction products is also provided in Fig. 7. These EDS spectra show that the chemical composition of gels for the different pastes varied slightly and that either both types of gels N-A-S-H and C-A-S-H are present in all AAFS paste or they are highly cross-linked (C-N-S-A-H) with each other. The formation of N-A-S-H gel along with the C-A-S-H gel for GGBS content of 20% has been also reported in the literature [51]. The possibility of a higher degree of cross-linking of both gel in AAFS pastes is proposed in the following study due to the presence of a higher amount of all major elements participating in the gel composition (Na, Ca, Si, and Al). Due to the higher Ca in HAP-16F and HAP-24F, both of these pastes show the presence of a slightly higher amount of Ca-rich C-(N)-A-S-H gel as compared to CP-0F and HAP-8F. The detailed discussion of chemical composition of reaction products and statistical analysis through BSE-EDS are provided in authors previous work [44].

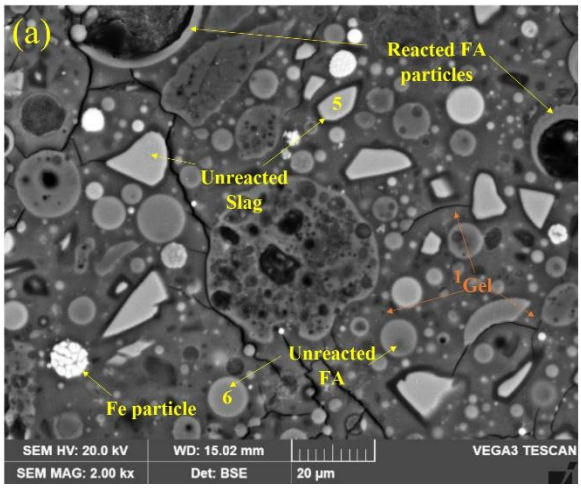
(a)
Reacted FA particles
5
Unreacted Slag
1 Gel
Unreacted FA
6
Fe particle
SEM HV: 20.0 kV
WD: 15.02 mm
VEGA3 TESCAN
SEM MAG: 2.00 kx
Det: BSE
20 µm

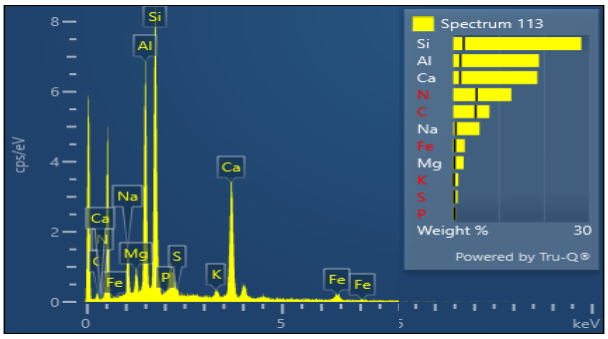
Spectrum 113
Si
Al
Ca
N
C
Na
Fe
Mg
K
S
P
Weight %
30
Powered by Tru-Q®
cps/eV
keV

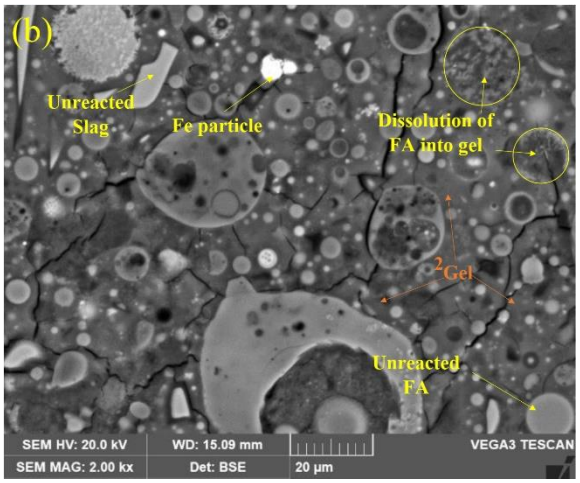
(b)
Unreacted Slag
Fe particle
Dissolution of FA into gel
2 Gel
Unreacted FA
SEM HV: 20.0 kV
WD: 15.09 mm
VEGA3 TESCAN
SEM MAG: 2.00 kx
Det: BSE
20 µm

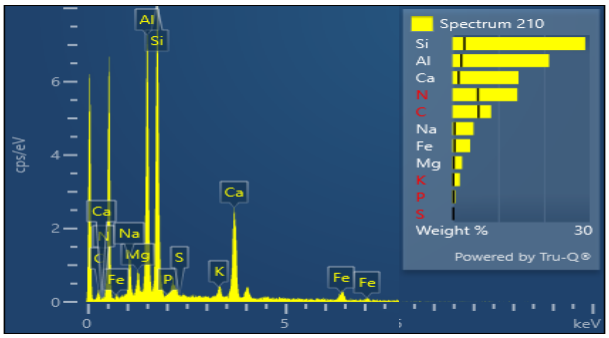
Spectrum 210
Si
Al
Ca
N
C
Na
Fe
Mg
K
P
S
Weight %
30
Powered by Tru-Q®
cps/eV
keV

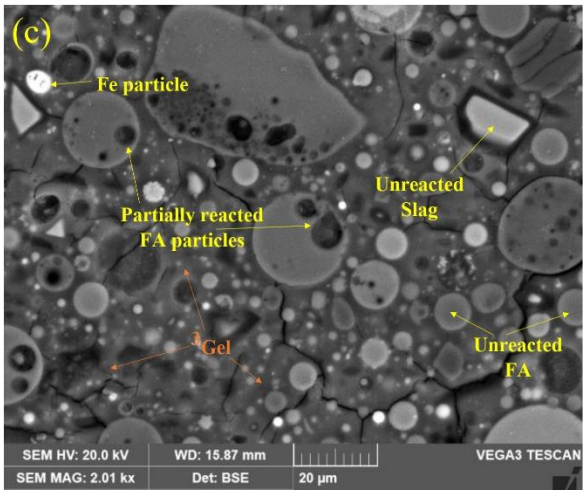
(c)
Fe particle
Unreacted Slag
Partially reacted FA particles
3 Gel
Unreacted FA
SEM HV: 20.0 kV
WD: 15.87 mm
VEGA3 TESCAN
SEM MAG: 2.01 kx
Det: BSE
20 µm

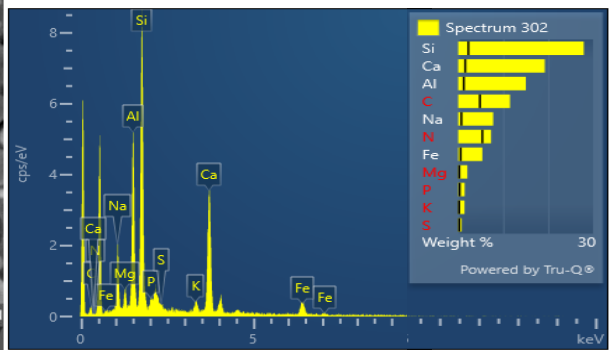
Spectrum 302
Si
Ca
Al
C
Na
N
Fe
Mg
P
K
S
Weight %
30
Powered by Tru-Q®
cps/eV
keV

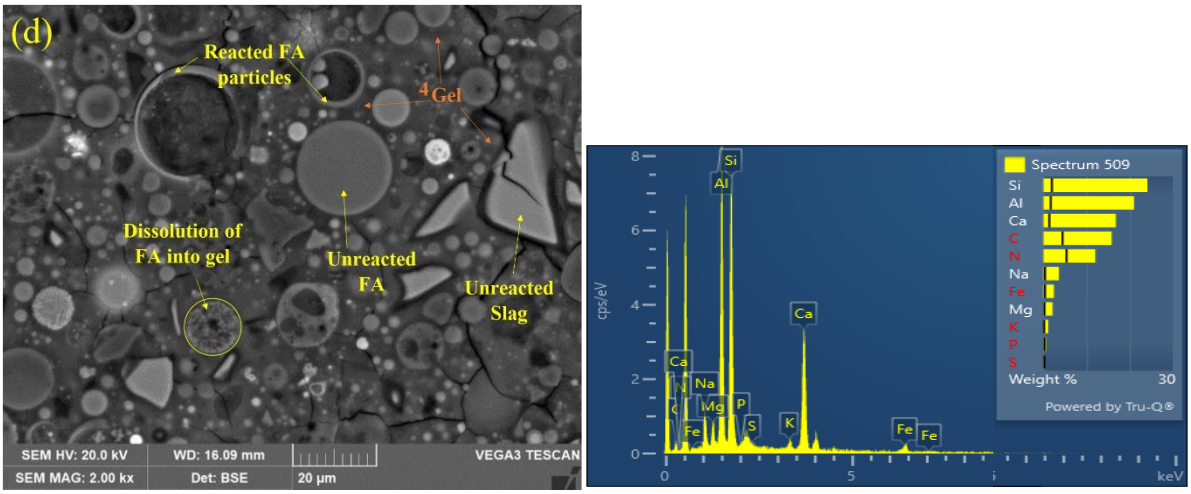

Fig. 7. SEM-BSE image and EDS spectra of AAFS pastes for (a) CP-0F; (b) HAP-8F; (c) HAP-16F and (d) HAP-24F

3.5 X-ray diffraction analysis of AAFS pastes.

XRD patterns of raw materials are provided in Fig. 8a. The main phases in FGR are thenardite (Na_2SO_4), monosodium phosphate (NaH_2PO_4) and trisodium phosphate (Na_3PO_4). FA mainly consists of quartz (SiO_2) and mullite ($3Al_2O_3{\cdot}2SiO_2$). A broad hump in GGBS is observed in the range of 25-35º 2θ showing its highly amorphous nature. XRD analysis on AAFS pastes was performed at 7 and 28 days to study the development of reaction products and results are presented in Fig. 8b and Fig.8c respectively. There are two distinct peaks (a sharp peak around 27° and a weak peak around 30°) in all AAFS pastes at 7 days. The peak at 30° is linked to the presence of calcite/reaction products ($CaCO_3$, C(A)-S-H) [54,55] which is formed as a result of a reaction of Ca (from GGBS) with tetrahedral silica $[SiO_4]^{4-}$ from the silica-based activator or raw precursors. Some of the aluminosilicate peaks present in the raw FA were absent in AAFS pastes indicating the dissolution of FA precursors to from the alkali-activated (C-A-S-H) and geopolymer gel (N-A-S-H). The dissolution of mullite and quartz in partial quantities has been reported by past studies as it helps to increase the strength of matrix by forming the amorphous silica gel [56]. However, the alkali-activated or geopolymer gel is difficult to identify using the results of XRD analysis due to their highly amorphous nature and coexistence with other crystalline phases [57]. The presence of a broad hump from 20° to 35° is observed at 7 days, similar to raw FA, which means that FA is not completely dissolved at 7

days. The XRD patterns of AAFS pastes at 28 days are similar to 7 days, however, intensity of unreacted phases is significantly reduced with the increase in time. This shows the partial dissolution of SiO_2 phases at a later age [58]. The broad hump around 20-35° present in raw FA and 7 days completely disappeared at 28 days which indicates that vitreous phases in FA have been dissolved to form the reaction products [59].

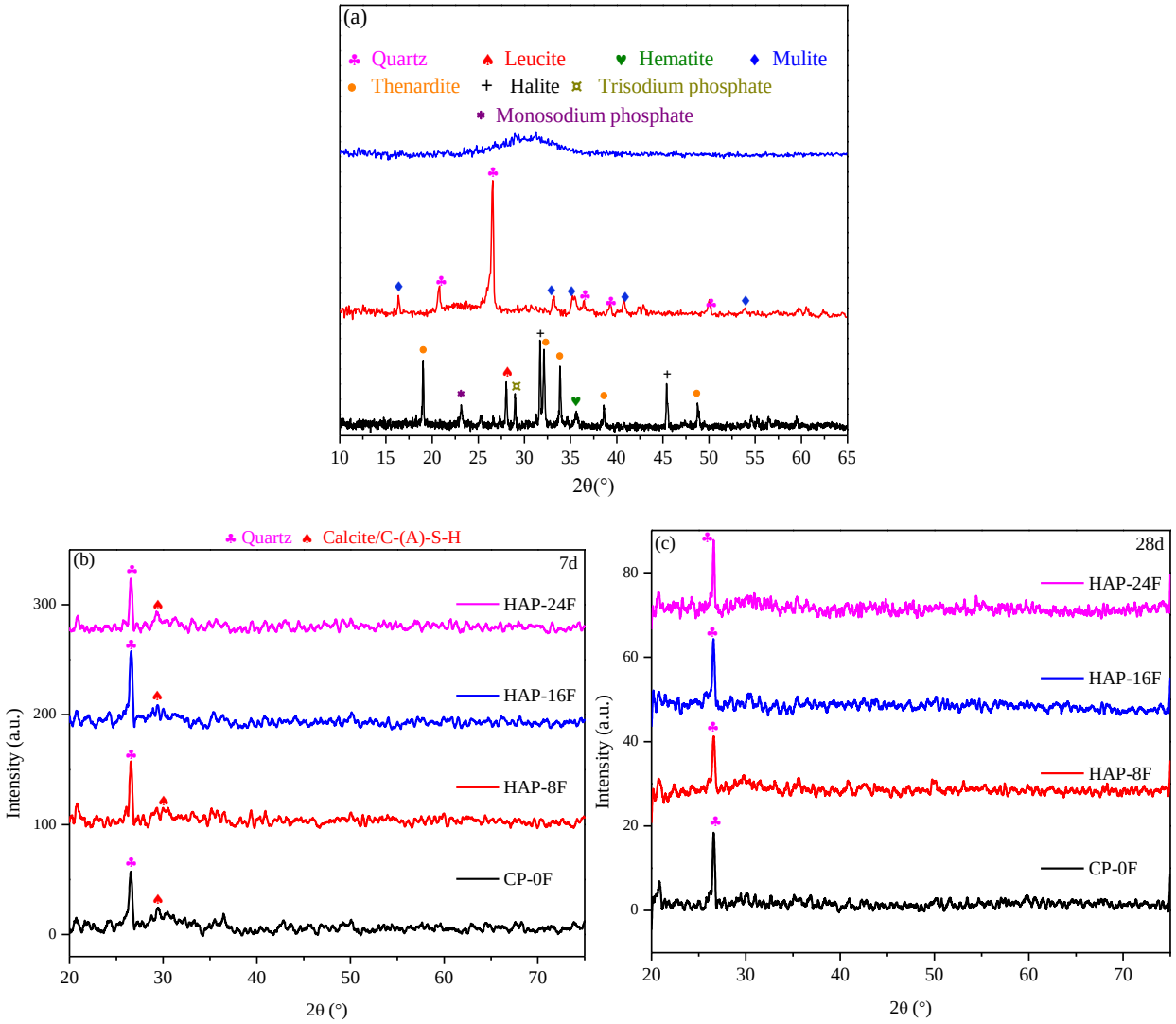

Fig. 8. XRD patterns of (a) raw materials, (b) AAFS pastes at 7 days and (c) AAFS pastes at 28 days

3.6 ^{29}Si MAS NMR analysis

The ^{29}Si MAS NMR spectra of AAFS paste powder are shown in Fig. 9. A broad hump is observed in all AAFS pastes in range of -80 to -110 ppm due to the presence of polymerized silicate species in large quantities. A relatively shorter hump is also observed in the range of -115 to 125 pm. These broad

resonances are indicative of the presence of amorphous reaction products in the AAFS pastes. The peak of broader hump (-80 to -110 ppm) is centered at -99 pm. The intensity of peak first increased for the paste containing 8% FGR (HAP-8F) and then decreased when CSS was further replaced by 16% and 24% FGR. However, the intensity of shorter hump was gradually increased with the increase in amount of FGR. This is associated with a higher amount of dissolution of Al species in Q^4(mAl) which can promote the formation of Q^4 structural units by transferring the Al-O-Si to Si-O-Si, hence, a slight modification in silicate structure occurs after FGR is introduced into AAFS pastes. The typical ^{29}Si NMR spectrum of FA shows a broad hump in the range of -80 to -120 ppm (centered at -110 pm) with the overlapped peaks [48,60]. The shift of hump to a higher frequency in pastes usually indicates the reaction extent of precursors due to an increase in the coordination of AlO_4 and SiO_4 and incorporation of Ca^{+2} and Na^+ to balance the AlO_4^- negative charge on the bridging oxygen in the coordinated AlO_4-O-SiO_4. The shift of main hump to the higher frequency is observed in all AAFS pastes showing the formation of Si species in the M-A-S-H gel. The shift of hump toward higher ppm is associated with the replacement of Si by Al in the first coordination sphere of primary Si atoms in 3D M-A-S-H gel network structure. The breadth and intensity of the main hump come from the contribution of the varying content of Q^4(mAl) overlapping species [47]. The relative quantities of these species are determined after deconvolution of ^{29}Si NMR spectra of AAFS pastes using the Gaussian distribution method.

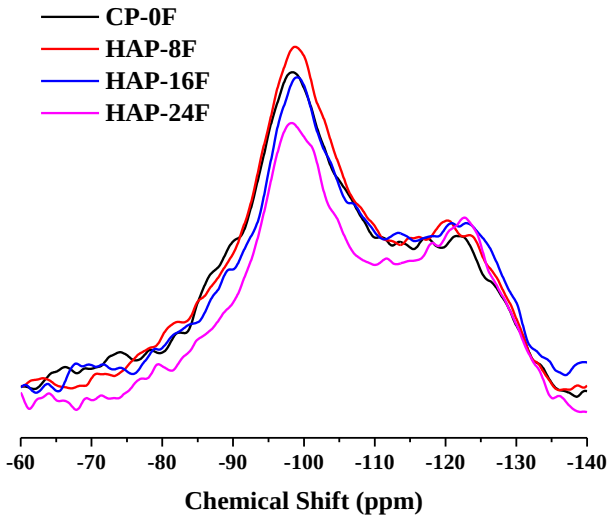

Fig. 9. The ^{29}Si MAS NMR spectra of AAFS paste powders

The original ^{29}Si NMR spectra for pastes, their fitted spectra, and associated deconvolutions are shown in Fig. 10. The ^{29}Si NMR spectral deconvolution for AAFS pastes consists of resonances at -66, -74, -82, -89, -99, -106, -113, -116, -123, -128 ppm [60–64]. The resonance around -66 is linked to the presence of Q^0 sites and is only found in the CP-0F and HAP-8F pastes in little quantities. The presence of this specie is due to monomer silicate structure from the dissolved precursors or remnant soluble silicate which has not taken part in the reaction. The Q^2 species (-74 ppm) are also observed but in significantly lower quantities in the CP-0F and HAP-16F. For the AAFS pastes, the resonances at -82, -89, -99, and -106 ppm are associated with the presence of Q^4(4Al), Q^4(3Al), Q^4(2Al), Q^4(1Al) species respectively. The resonances after -106 ppm are associated with the Q^4(0Al) species. It is to be noted that some structural units may correspond to several chemical shift peaks and hence they are separated into multiple shifts for improved curve fitting [60,62,65].

The results of deconvolution peaks are quantified by calculating the area of each peak and presented in Fig. 11. The amount of Q^0 and Q^2 species is very low in all AAFS pastes. The 3D gel network of AAFS pastes is dominated by the Q^4(mAl) species (m = 0, 1, 2, 3, and 4). The content of Q^4(0Al) was higher in HAP-16F (40.4%) and HAP-24F (42.1%) as compared to CP-0F (36.9%) and HAP-8F (31.6%). The content of Q^4(1Al) was also higher in the pastes containing FGR as compared to control paste (CP-0F). However, a higher amount of Q^4(2Al) structural units is observed in control pastes than that of HAPs. The amount of Q^4(3Al) was highest for HAP-8F (17.2%). A relatively lower quantity of Q^4(4Al) was found in the CP-0F, HAP-16F, and HAP-24F as compared to other Q^4 species. Based on the results, the reaction of the silicate units in AAFS pastes can be described as follows. The increase in the content of FGR (higher alkaline environment) could result in increasing the content of low-aluminite silicate species (Q^4(0Al) and Q^4(1Al)) and decreasing the content of high-aluminate silicate species (Q^4(3Al) and Q^4(4Al)). The higher amount of dealumination of Q^4(mAl) species from aluminosilicate precursor promotes the silicon tetrahedrons condensation which can lead to an increase in the content of Q^4(0Al) species in pastes containing a higher

amount of FGR. The higher amount of formation of Q^4(0Al) species is linked with the higher compressive of geopolymer-based materials [65].

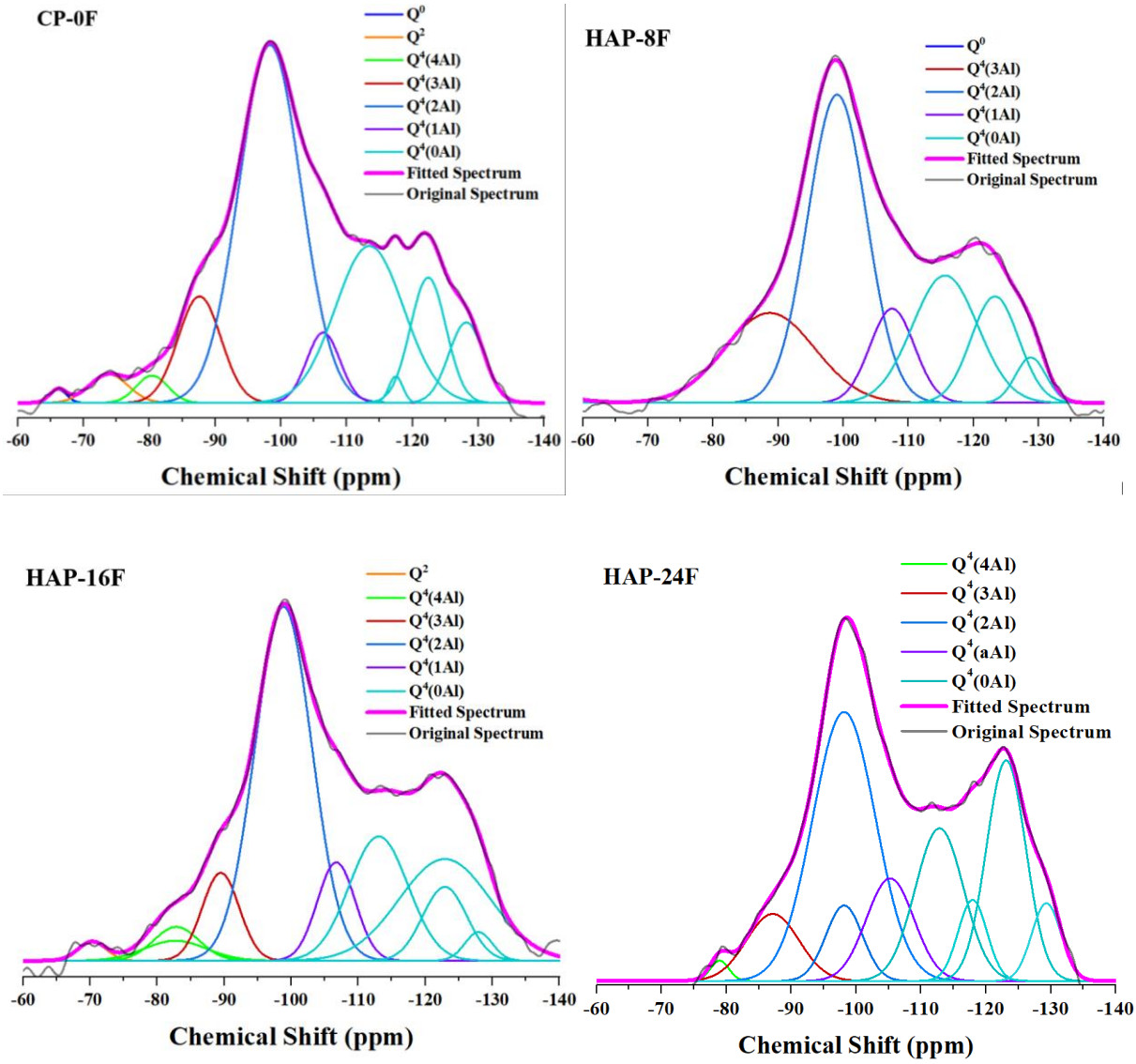

Fig. 10. Spectral Deconvolution of AAFS paste powders for ^{29}Si MAS NMR

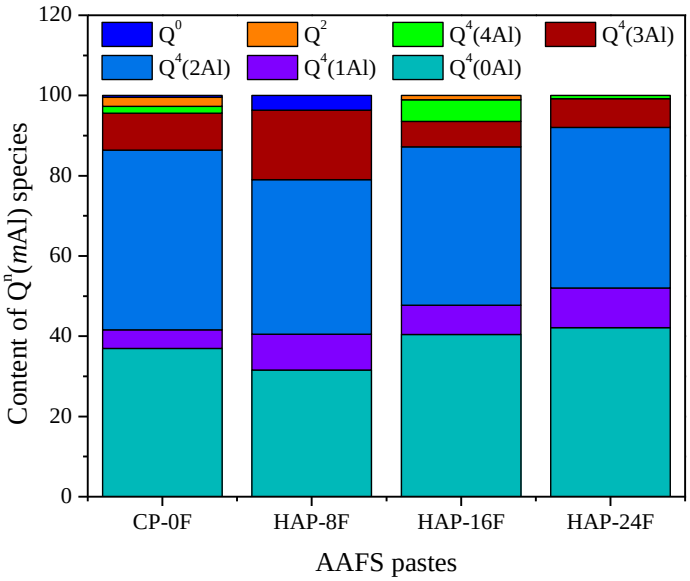

Fig. 11. Quantification of silicate structural units in each AAFS paste

4 Conclusions:

In this study, FGR and CSS were utilized as a hybrid activator to produce the AAFS pastes. Characterization of AAFS pastes was conducted by selective dissolution, XRF, TGA, SEM, and NMR analysis techniques. Based on the results, the following conclusions are drawn:

1. Selective dissolution by SAM showed that a higher amount of C-A-S-H gel was formed in HAP-24F followed by HAP-16F, CP-0F, and HAP-8F. HCL dissolution indicated the higher amount of formation of N-A-S-H in CP-0F followed by HAP-16F, HAP-24F, and HAP-8F.
2. The chemical composition of residues determined by XRF analysis showed that amount of CaO and Na_2O was significantly reduced as compared to original pastes confirming the dissolution of C-A-S-H and N-A-S-H by HCl and SAM treatment. The increase in the amount of SiO_2 and Al_2O_3 of residues after selective dissolution was due to the presence of unreacted FA left in paste residues. SEM-EDS analysis on the HCl and SAM residues also showed similar results as the percentage of Na and Ca was greatly reduced after selective dissolution.
3. The TGA analysis of original pastes powder showed that amount of reaction products was slightly increased with the increase in amount of FGR. TGA analysis of SAM residues

indicated that a slightly higher amount of N-A-S-H gel was formed in CP-0F as compared to HAP pastes which also corroborated the SEM-EDS results.

4. SEM-EDS point analysis on AAFS pastes residues before and after selective dissolution confirmed the formation of different types of reaction products (N-A-S-H, C-A-S-H and C-N-A-S-H).
5. The ^{29}Si MAS NMR analysis of AAFS pastes indicated that the quantity of Q^4(0Al) and Q^4(1Al) structural units were increased when amount of FGR was gradually increased from 0% to 24% however, an opposite trend was observed for the Q^4(3Al) and Q^4(4Al) structural units.

Acknowledgments

The authors would like to acknowledge the financial support received from NSFC/RGC Joint Research Scheme (N_PolyU542/20), Hong Kong RGC General Research Fund (No. 15223120), The Hong Kong Polytechnic University through the Post-doctoral Fellowship (1-W16R) the Research Institute for Sustainable Urban Development (No.1-BBWE). We also gratefully acknowledge the support of the University Research Facility on Chemical and Environmental Analysis (UCEA) of PolyU.

References:

[1] B.C. McLellan, R.P. Williams, J. Lay, A. van Riessen, G.D. Corder, Costs and carbon emissions for geopolymer pastes in comparison to ordinary portland cement, J Clean Prod. 19 (2011) 1080–1090. https://doi.org/https://doi.org/10.1016/j.jclepro.2011.02.010.

[2] A. Passuello, E.D. Rodríguez, E. Hirt, M. Longhi, S.A. Bernal, J.L. Provis, A.P. Kirchheim, Evaluation of the potential improvement in the environmental footprint of geopolymers using waste-

derived activators, J Clean Prod. 166 (2017) 680–689. https://doi.org/https://doi.org/10.1016/j.jclepro.2017.08.007.

[3] M.R. Ahmad, B. Chen, S.F.A. Shah, Influence of different admixtures on the mechanical and durability properties of one-part alkali-activated mortars, Constr Build Mater. 265 (2020) 120320. https://doi.org/10.1016/J.CONBUILDMAT.2020.120320.

[4] Z. Pan, L. Cheng, Y. Lu, N. Yang, Hydration products of alkali-activated slag–red mud cementitious material, Cem Concr Res. 32 (2002) 357–362. https://doi.org/https://doi.org/10.1016/S0008-8846(01)00683-4.

[5] M.R. Ahmad, B. Chen, S.F.A. Shah, Influence of different admixtures on the mechanical and durability properties of one-part alkali-activated mortars, Constr Build Mater. 265 (2020) 120320. https://doi.org/10.1016/j.conbuildmat.2020.120320.

[6] S. Yousefi Oderji, B. Chen, M.R. Ahmad, S.F.A. Shah, Fresh and hardened properties of one-part fly ash-based geopolymer binders cured at room temperature: Effect of slag and alkali activators, J Clean Prod. 225 (2019) 1–10. https://doi.org/10.1016/j.jclepro.2019.03.290.

[7] F. Collins, J.G. Sanjayan, Effects of ultra-fine materials on workability and strength of concrete containing alkali-activated slag as the binder, Cem Concr Res. 29 (1999) 459–462. https://doi.org/https://doi.org/10.1016/S0008-8846(98)00237-3.

[8] M. Komljenović, Z. Baščarević, V. Bradić, Mechanical and microstructural properties of alkali-activated fly ash geopolymers, J Hazard Mater. 181 (2010) 35–42. https://doi.org/https://doi.org/10.1016/j.jhazmat.2010.04.064.

[9] B. Walkley, R. San Nicolas, M.-A. Sani, G.J. Rees, J. v Hanna, J.S.J. van Deventer, J.L. Provis, Phase evolution of C-(N)-A-S-H/N-A-S-H gel blends investigated via alkali-activation of synthetic calcium aluminosilicate precursors, Cem Concr Res. 89 (2016) 120–135. https://doi.org/https://doi.org/10.1016/j.cemconres.2016.08.010.

[10] S.A. Bernal, J.L. Provis, B. Walkley, R. San Nicolas, J.D. Gehman, D.G. Brice, A.R. Kilcullen, P. Duxson, J.S.J. van Deventer, Gel nanostructure in alkali-activated binders based on slag and fly ash, and effects of accelerated carbonation, Cem Concr Res. 53 (2013) 127–144. https://doi.org/https://doi.org/10.1016/j.cemconres.2013.06.007.

[11] P. Perez-Cortes, J.I. Escalante-Garcia, Gel composition and molecular structure of alkali-activated metakaolin-limestone cements, Cem Concr Res. 137 (2020) 106211. https://doi.org/https://doi.org/10.1016/j.cemconres.2020.106211.

[12] S. Puligilla, P. Mondal, Co-existence of aluminosilicate and calcium silicate gel characterized through selective dissolution and FTIR spectral subtraction, Cem Concr Res. 70 (2015) 39–49.

[13] Z. Giergiczny, Fly ash and slag, Cem Concr Res. 124 (2019) 105826. https://doi.org/https://doi.org/10.1016/j.cemconres.2019.105826.

[14] Y. Li, Y. Sun, Preliminary study on combined-alkali–slag paste materials, Cem Concr Res. 30 (2000) 963–966. https://doi.org/https://doi.org/10.1016/S0008-8846(00)00269-6.

[15] F. Winnefeld, A. Leemann, M. Lucuk, P. Svoboda, M. Neuroth, Assessment of phase formation in alkali activated low and high calcium fly ashes in building materials, Constr Build Mater. 24 (2010) 1086–1093. https://doi.org/https://doi.org/10.1016/j.conbuildmat.2009.11.007.

[16] A. Buchwald, M. Schulz, Alkali-activated binders by use of industrial by-products, Cem Concr Res. 35 (2005) 968–973. https://doi.org/https://doi.org/10.1016/j.cemconres.2004.06.019.

[17] Y. Alrefaei, Y.S. Wang, J.G. Dai, The effectiveness of different superplasticizers in ambient cured one-part alkali activated pastes, Cem Concr Compos. 97 (2019) 166–174. https://doi.org/10.1016/J.CEMCONCOMP.2018.12.027.

[18] Y.S. Wang, Y. Alrefaei, J.G. Dai, Roles of hybrid activators in improving the early-age properties of one-part geopolymer pastes, Constr Build Mater. 306 (2021) 124880. https://doi.org/10.1016/J.CONBUILDMAT.2021.124880.

[19] M. Fawer, M. Concannon, W. Rieber, Life cycle inventories for the production of sodium silicates, Int J Life Cycle Assess. 4 (1999) 207. https://doi.org/10.1007/BF02979498.

[20] R. Bajpai, K. Choudhary, A. Srivastava, K.S. Sangwan, M. Singh, Environmental impact assessment of fly ash and silica fume based geopolymer concrete, J Clean Prod. 254 (2020) 120147. https://doi.org/https://doi.org/10.1016/j.jclepro.2020.120147.

[21] G. di Bella, I. Arrigo, P. Catalfamo, F. Corigliano, L. Mavilia, Advances in the extraction of silica from glass cullet, in: Recycling and Reuse of Waste Materials, Thomas Telford Publishing, 2003: pp. 137–142.

[22] F. Puertas, M. Torres-Carrasco, Use of glass waste as an activator in the preparation of alkali-activated slag. Mechanical strength and paste characterisation, Cem Concr Res. 57 (2014) 95–104. https://doi.org/https://doi.org/10.1016/j.cemconres.2013.12.005.

[23] M. Torres-Carrasco, F. Puertas, Waste glass in the geopolymer preparation. Mechanical and microstructural characterisation, J Clean Prod. 90 (2015) 397–408. https://doi.org/https://doi.org/10.1016/j.jclepro.2014.11.074.

[24] I. Bianco, B. Ap Dafydd Tomos, R. Vinai, Analysis of the environmental impacts of alkali-activated concrete produced with waste glass-derived silicate activator – A LCA study, J Clean Prod. 316 (2021) 128383. https://doi.org/https://doi.org/10.1016/j.jclepro.2021.128383.

[25] H. MORI, Extraction of Silicon Dioxide from Waste Colored Glasses by Alkali Fusion Using Sodium Hydroxide, Journal of the Ceramic Society of Japan. 111 (2003) 376–381. https://doi.org/10.2109/jcersj.111.376.

[26] M. Keawthun, S. Krachodnok, A. Chaisena, Conversion of waste glasses into sodium silicate solutions, International Journal of Chemical Sciences. 12 (2014) 83–91. https://www.scopus.com/inward/record.uri?eid=2-s2.0-84896387397&partnerID=40&md5=0781919075a282f402202d83f1a87d76.

[27] B. Hu, S. Zhao, S. Zhang, Removal of lead from cathode ray tube funnel glass by generating the sodium silicate, J Air Waste Manage Assoc. 65 (2015) 106–114. https://doi.org/10.1080/10962247.2014.976721.

[28] R. Vinai, M. Soutsos, Production of sodium silicate powder from waste glass cullet for alkali activation of alternative binders, Cem Concr Res. 116 (2019) 45–56. https://doi.org/https://doi.org/10.1016/j.cemconres.2018.11.008.

[29] A. Fernández-Jiménez, N. Cristelo, T. Miranda, Á. Palomo, Sustainable alkali activated materials: Precursor and activator derived from industrial wastes, J Clean Prod. 162 (2017) 1200–1209. https://doi.org/https://doi.org/10.1016/j.jclepro.2017.06.151.

[30] A. Maldonado-Alameda, J. Giro-Paloma, A. Rodríguez-Romero, J. Serret, A. Menargues, A. Andrés, J.M. Chimenos, Environmental potential assessment of MSWI bottom ash-based alkali-activated binders, J Hazard Mater. 416 (2021) 125828. https://doi.org/https://doi.org/10.1016/j.jhazmat.2021.125828.

[31] J.C.B. Moraes, A. Font, L. Soriano, J.L. Akasaki, M.M. Tashima, J. Monzó, M. v Borrachero, J. Payá, New use of sugar cane straw ash in alkali-activated materials: A silica source for the preparation of the alkaline activator, Constr Build Mater. 171 (2018) 611–621. https://doi.org/https://doi.org/10.1016/j.conbuildmat.2018.03.230.

[32] R. Vinai, M. Soutsos, Production of sodium silicate powder from waste glass cullet for alkali activation of alternative binders, Cem Concr Res. 116 (2019) 45–56.

[33] M.F. Alnahhal, A. Hamdan, A. Hajimohammadi, T. Kim, Effect of rice husk ash-derived activator on the structural build-up of alkali activated materials, Cem Concr Res. 150 (2021) 106590. https://doi.org/https://doi.org/10.1016/j.cemconres.2021.106590.

[34] (Environmental Protection Department) EPD, Integrated Waste Management Facilities, Problems & Solutions, (2021). https://www.epd.gov.hk/epd/english/environmentinhk/waste/prob_solutions/WFdev_IWMF.html (accessed September 30, 2022).

[35] M.R. Ahmad, J. Lao, J.-G. Dai, D. Xuan, C.S. Poon, Upcycling of air pollution control residue waste into cementitious product through geopolymerization technology, Resour Conserv Recycl. 181 (2022) 106231. https://doi.org/10.1016/J.RESCONREC.2022.106231.

[36] A. Bogush, J.A. Stegemann, I. Wood, A. Roy, Element composition and mineralogical characterisation of air pollution control residue from UK energy-from-waste facilities, Waste Management. 36 (2015) 119–129. https://doi.org/https://doi.org/10.1016/j.wasman.2014.11.017.

[37] A.J. Chandler, T.T. Eighmy, O. Hjelmar, D.S. Kosson, S.E. Sawell, J. Vehlow, H.A. van der Sloot, J. Hartlén, Municipal solid waste incinerator residues, Elsevier, 1997.

[38] J.A. Stegemann, The potential role of energy-from-waste air pollution control residues in the industrial ecology of cement, J Sustain Cem Based Mater. 3 (2014) 111–127.

[39] M.J. Quina, J.M. Bordado, R.M. Quinta-Ferreira, Recycling of air pollution control residues from municipal solid waste incineration into lightweight aggregates, Waste Management. 34 (2014) 430–438. https://doi.org/https://doi.org/10.1016/j.wasman.2013.10.029.

[40] A.A. Bogush, J.A. Stegemann, Q. Zhou, Z. Wang, B. Zhang, T. Zhang, W. Zhang, J. Wei, Co-processing of raw and washed air pollution control residues from energy-from-waste facilities in the cement kiln, J Clean Prod. 254 (2020) 119924. https://doi.org/https://doi.org/10.1016/j.jclepro.2019.119924.

[41] K. I., A.R. D., B.A. R., C.C. R., Geopolymers from DC Plasma–Treated Air Pollution Control Residues, Metakaolin, and Granulated Blast Furnace Slag, Journal of Materials in Civil Engineering. 23 (2011) 735–740. https://doi.org/10.1061/(ASCE)MT.1943-5533.0000170.

[42] I. Kourti, D.A. Rani, D. Deegan, A.R. Boccaccini, C.R. Cheeseman, Production of geopolymers using glass produced from DC plasma treatment of air pollution control (APC) residues, J Hazard Mater. 176 (2010) 704–709. https://doi.org/https://doi.org/10.1016/j.jhazmat.2009.11.089.

[43] R. Shirley, L. Black, Alkali activated solidification/stabilisation of air pollution control residues and co-fired pulverised fuel ash, J Hazard Mater. 194 (2011) 232–242. https://doi.org/https://doi.org/10.1016/j.jhazmat.2011.07.100.

[44] M.R. Ahmad, L.P. Qian, Y. Fang, A. Wang, J.G. Dai, A multiscale study on gel composition of hybrid alkali-activated materials partially utilizing air pollution control residue as an activator, Cem Concr Compos. 136 (2023) 104856. https://doi.org/10.1016/J.CEMCONCOMP.2022.104856.

[45] J. Fu, M.W. Bligh, I. Shikhov, A.M. Jones, C. Holt, L.M. Keyte, F. Moghaddam, C.H. Arns, S.J. Foster, T.D. Waite, A microstructural investigation of a Na2SO4 activated cement-slag blend, Cem Concr Res. 150 (2021) 106609. https://doi.org/https://doi.org/10.1016/j.cemconres.2021.106609.

[46] Y. Alrefaei, Y.-S. Wang, J.-G. Dai, Q.-F. Xu, Effect of superplasticizers on properties of one-part Ca(OH)2/Na2SO4 activated geopolymer pastes, Constr Build Mater. 241 (2020) 117990. https://doi.org/https://doi.org/10.1016/j.conbuildmat.2019.117990.

[47] M.A. Longhi, B. Walkley, E.D. Rodríguez, A.P. Kirchheim, Z. Zhang, H. Wang, New selective dissolution process to quantify reaction extent and product stability in metakaolin-based geopolymers, Compos B Eng. 176 (2019) 107172. https://doi.org/https://doi.org/10.1016/j.compositesb.2019.107172.

[48] N.K. Lee, H.-K. Lee, Reactivity and reaction products of alkali-activated, fly ash/slag paste, Constr Build Mater. 81 (2015) 303–312.

[49] S. Zhang, A. Keulen, K. Arbi, G. Ye, Waste glass as partial mineral precursor in alkali-activated slag/fly ash system, Cem Concr Res. 102 (2017) 29–40. https://doi.org/https://doi.org/10.1016/j.cemconres.2017.08.012.

[50] X. Dai, S. Aydın, M.Y. Yardımcı, K. Lesage, G. de Schutter, Effects of activator properties and GGBFS/FA ratio on the structural build-up and rheology of AAC, Cem Concr Res. 138 (2020) 106253. https://doi.org/https://doi.org/10.1016/j.cemconres.2020.106253.

[51] A. Rafeet, R. Vinai, M. Soutsos, W. Sha, Effects of slag substitution on physical and mechanical properties of fly ash-based alkali activated binders (AABs), Cem Concr Res. 122 (2019) 118–135. https://doi.org/https://doi.org/10.1016/j.cemconres.2019.05.003.

[52] I. Hager, M. Sitarz, K. Mróz, Fly-ash based geopolymer mortar for high-temperature application – Effect of slag addition, J Clean Prod. 316 (2021) 128168. https://doi.org/https://doi.org/10.1016/j.jclepro.2021.128168.

[53] J.C. Kuri, S. Majhi, P.K. Sarker, A. Mukherjee, Microstructural and non-destructive investigation of the effect of high temperature exposure on ground ferronickel slag blended fly ash geopolymer mortars, Journal of Building Engineering. 43 (2021) 103099. https://doi.org/https://doi.org/10.1016/j.jobe.2021.103099.

[54] F.A. Ababneh, A.I. Alakhras, M. Heikal, S.M. Ibrahim, Stabilization of lead bearing sludge by utilization in fly ash-slag based geopolymer, Constr Build Mater. 227 (2019) 116694.

[55] M.R. Ahmad, B. Chen, S.F. Ali Shah, Mechanical and microstructural characterization of bio-concrete prepared with optimized alternative green binders, Constr Build Mater. 281 (2021) 122533. https://doi.org/https://doi.org/10.1016/j.conbuildmat.2021.122533.

[56] Y. Li, J. Li, J. Cui, Y. Shan, Y. Niu, Experimental study on calcium carbide residue as a combined activator for coal gangue geopolymer and feasibility for soil stabilization, Constr Build Mater. 312 (2021) 125465. https://doi.org/https://doi.org/10.1016/j.conbuildmat.2021.125465.

[57] H. Xu, W. Gong, L. Syltebo, K. Izzo, W. Lutze, I.L. Pegg, Effect of blast furnace slag grades on fly ash based geopolymer waste forms, Fuel. 133 (2014) 332–340.

[58] P.N. Lemougna, U.F. Chinje Melo, M.P. Delplancke, H. Rahier, Influence of the chemical and mineralogical composition on the reactivity of volcanic ashes during alkali activation, Ceram Int. 40 (2014) 811–820. https://doi.org/10.1016/J.CERAMINT.2013.06.072.

[59] C. Lu, Q. Wang, Y. Liu, T. Xue, Q. Yu, S. Chen, Influence of new organic alkali activators on microstructure and strength of fly ash geopolymer, Ceram Int. (2022). https://doi.org/10.1016/J.CERAMINT.2022.01.109.

[60] X. Gao, Q.L. Yu, H.J.H. Brouwers, Apply 29Si, 27Al MAS NMR and selective dissolution in identifying the reaction degree of alkali activated slag-fly ash composites, Ceram Int. 43 (2017) 12408–12419. https://doi.org/https://doi.org/10.1016/j.ceramint.2017.06.108.

[61] W.J. Malfait, W.E. Halter, R. Verel, 29Si NMR spectroscopy of silica glass: T1 relaxation and constraints on the Si–O–Si bond angle distribution, Chem Geol. 256 (2008) 269–277. https://doi.org/10.1016/J.CHEMGEO.2008.06.048.

[62] S.A. Bernal, J.L. Provis, B. Walkley, R. San Nicolas, J.D. Gehman, D.G. Brice, A.R. Kilcullen, P. Duxson, J.S.J. van Deventer, Gel nanostructure in alkali-activated binders based on slag and fly ash, and effects of accelerated carbonation, Cem Concr Res. 53 (2013) 127–144. https://doi.org/10.1016/J.CEMCONRES.2013.06.007.

[63] I.G. Richardson, The calcium silicate hydrates, Cem Concr Res. 38 (2008) 137–158. https://doi.org/10.1016/J.CEMCONRES.2007.11.005.

[64] B. Walkley, R. San Nicolas, M.A. Sani, J.D. Gehman, J.S.J. van Deventer, J.L. Provis, Phase evolution of Na2O–Al2O3–SiO2–H2O gels in synthetic aluminosilicate binders, Dalton Transactions. 45 (2016) 5521–5535. https://doi.org/10.1039/C5DT04878H.

[65] H. Lin, H. Liu, Y. Li, X. Kong, Properties and reaction mechanism of phosphoric acid activated metakaolin geopolymer at varied curing temperatures, Cem Concr Res. 144 (2021) 106425. https://doi.org/https://doi.org/10.1016/j.cemconres.2021.106425.